Chinese Journal of
POLYMER SCIENCE

RESEARCH ARTICLE

https://doi.org/10.1007/s10118-024-3151-3
Chinese J. Polym. Sci. **2024**, *42*, 1368–1374

Friction between Strongly Compressed Polymer Brushes

Qi Liao*

Institute of Chemistry, Chinese Academy of Sciences, Beijing 100190, China

Abstract We present the results of molecular dynamics simulations of steady shear between a pair of neutral polymer brushes, as well as a pair of charged polymer brushes in the strongly compressed regime. The results of the molecular dynamic simulations of neutral and polyelectrolyte brushes in implicit solvent including normal forces, shear forces, viscosities and friction coefficients as a function of separation between brushes, are presented in the study. The comparison of the simulation results of neutral and charged brushes shows that the charged brushes is in the quasi-neutral regime, and the dependence of viscosity on the separation distance show the similar power law of neutral brushes. Our simulation results confirm that the implicit solvent simulations of polyelectrolyte brushes that ignore hydrodynamics interaction are in agreement with the scaling predictions qualitatively because of screening of hydrodynamic interaction and long-range electrostatic interactions on the correlation length scale. Both of neutral and charged brushes show the lubrication properties that the friction coefficient decreases with the separation decreases at enough large loads. However, a maximum of friction coefficients is observed for polyelectrolyte brushes, which is in contrast to the neutral brushes with monotonical dependence.

Keywords Polymer brush; Frictions coefficient; Polyelectrolyte; Lubrication

Citation: Liao, Q. Friction between strongly compressed polymer brushes. *Chinese J. Polym. Sci.* **2024**, *42*, 1368–1374.

INTRODUCTION

A polymer brush is formed by grafted polymer chains that extend away from the surface due to interchain repulsion at high grafting density.[1] Polymer brushes are of high utility in friction and bio-lubrication of biological systems.[2] Lubrication properties of polymer brushes have been extensively studied experimentally,[3,4] theoretically[5,6] and by computer simulations.[7,8] Friction coefficients (ratio of shear forces to the normal forces) between two polyelectrolyte brushes were measured to be much lower than between neutral brushes at similar polymer volume fraction in the gap between surfaces. This friction coefficient is expected to strongly depend on the interpenetration between the two brushes. However, it is difficult to experimentally measure this interpenetration. Interpenetration between brushes, in addition to shear and normal forces, can be directly obtained by computer simulations. Therefore, computer simulation is an excellent tool to elucidate structural and dynamical properties of both neutral and polyelectrolyte brushes.

Compression of two polymer brushes causes interpenetration of their chain sections. The main contribution to the shear forces between two brushes sliding past each other is from the friction experienced by chains as they are dragged through the interpenetration region. Hehmeyer *et al*. observed that the normal force f_N between polyelectrolyte brushes increased with decreasing separation D between plates as $f_N \sim D^{-\alpha}$.[9] The scaling exponent α increases from 0.7 to 2 with increasing grafting density in their simulations of short polyelectrolyte chains. Kumar *et al*. extended the simulations and reported the scaling relation of the separation dependence of the normal pressures as scaling exponent α=2 and 3 at different grafting densities.[10] Ou *et al*. observed lower friction coefficients between charged brushes in comparison to neutral brushes in their molecular dynamic simulations.[8] Their simulation results qualitatively show a lower friction coefficient for the charged brushes. Dobrynin's group reported the simulations of charged bottle-brushes and similar dependence of normal pressure on the separation with nonlinear scaling exponent α=1.8 is observed.[11] The comparison of neutral and charged bottle-brushes was also reported by Dobrynin's group in a more quantitative way. They have found that the friction coefficient between charged bottle-brushes is about ten times smaller than that between neutral systems at the same shear rate.

The molecular dynamics simulations of neutral brushes in explicit solvents were performed by Galuschko *et al*. The simulation reveals a crossover from linear response and non-linear response to the shear rate and the solvent effect plays an important role in the non-linear response regime with higher shear rate.[12] Using dissipative particle dynamics (DPD) simulations, Tildesley's group reported the results of compressed polyelectrolyte brushes with hydrodynamics interactions.[13] Their results show the capability of the DPD method to simulate the friction coefficients between a pair of polyelectrolyte brushes in wide separation range from far away separated brushes to strongly compressed brushes.

The focus of the present study is to study shear between

* Corresponding author, E-mail: qiliao@iccas.ac.cn

Special Issue: Charged Polymers
Received March 9, 2024; Accepted April 28, 2024; Published online June 5, 2024

strongly-compressed neutral and polyelectrolyte brushes and compare the results of the simulations with theoretical predictions. The work is organized as follows. The simulation model and methods are described in section **SIMULATION MODEL AND METHOD**. In section **RESULTS AND DISCUSSION** we present results of the molecular dynamic simulations of neutral and polyelectrolyte brushes in implicit solvent including normal forces, shear forces, viscosities and frictions coefficients as a function of separation between plates. Note that in the semidilute regime the hydrodynamic interactions are screened at the correlation length scale, thus the implicit solvent simulations provide a reasonable approaching of physical dynamics.[14] The comparison of the simulation results to the scaling predictions are also discussed in the section. Finally in section **CONCLUSIONS** we summarize our results.

SIMULATION MODEL AND METHOD

The brush is represented by an ensemble of M freely joined bead-spring chains of N+1 monomers, which are anchored at one end to an uncharged planar surface. The size of the simulation box is $L \times L \times L_Z$ and the grafting density is denoted by $\rho_a = M/L^2$. In our simulations of neutral and charged brushes, $L = 15\sigma$ and M=25, thus the grafting density ρ_a is fixed at $0.11\sigma^{-2}$. The uncharged anchor monomers are fixed and form a square lattice with lattice spacing $\rho_a^{-1/2}$. The simulation box is periodic in x and y directions, while perpendicular to the grafting surface the system is restricted to one layer. The fraction of charged monomers is given by $f = N_C/N = 1/3$, where N_C is the number of charged monomers per chain. Charged monomers are monovalent and spaced by $1/f$ monomers along the chain backbone. Since the solution is electro-neutral there are also $f\,N\,M$ counterions. Table 1 gives the list of the parameters used in our simulations, where V is the sliding velocity of the brush with respect to the other and l_B is the Bjerrum length. For the neural brushed, N=20 and for the charged brushes, N=40. Fig. 1 show the snapshots of neutral and charged brushes, respectively.

The chains are assumed to be in a good solvent and are modeled by a purely repulsive short-range interaction that is described by a shifted and truncated Lennard-Jones (LJ) potential U_{LJ}^S:

$$U_{LJ}^S(r) = \begin{cases} 4\varepsilon_{LJ}\left[\left(\frac{\sigma}{r}\right)^{12} - \left(\frac{\sigma}{r}\right)^{6}\right] + \varepsilon_{LJ}, & r \leqslant 2^{1/6}\sigma \\ 0, & r > 2^{1/6}\sigma \end{cases} \quad (1)$$

The same shifted LJ potential is also used to describe the purely repulsive excluded-volume interaction between any pair of counterions and between a monomer and a counterion. The LJ parameters ε_{LJ} and σ were chosen to be the same for the monomers and counterions. The connectivity of the monomers in the chains is maintained by a finitely extensible nonlinear elastic (FENE) potential:

$$U_{FENE}(r) = -\frac{1}{2}kR_0^2 \ln\left(1 - \frac{r^2}{R_0^2}\right) \quad (2)$$

where $k = 30\varepsilon_{LJ}\sigma^2$ is the spring constant and $R_0 = 1.5\sigma$ is the maximum bond length at which the elastic energy of bond becomes infinite. The FENE potential only gives the attractive part of the bond potential. The repulsive part of the bond potential is provided by the LJ interaction (Eq. 1).

All particles except the anchor monomers are repelled from both grafted surfaces (at $z = \pm D/2$) by a short-range repulsive interaction:

$$U_{Wall}(z) = A\left(\frac{\sigma}{D/2 - |z|}\right)^6, \frac{D}{2} - r_{cut} < |z| < \frac{D}{2} \quad (3)$$

where $A = 0.001\varepsilon_{LJ}$, and σ is the LJ length defined in Eq. (1). This repulsive interaction potential is cut off at the distance $r_{cut} = 0.4\sigma$ from the wall, as given in Eq. (3).

Solvent molecules are not included explicitly in the simulations. The solvent is modeled by a dielectric medium with the dielectric constant ε. In such continuous representation of the solvent, all charged particles interact with each other via unscreened Coulomb potential

Table 1 Simulation parameters for two charged brushes.

N	M	l_B/σ	L/σ	f	$V\tau_{LJ}/\sigma$	$\rho_n\sigma^2$
20 (neutral), 40 (charged)	25	1	15	1/3	0.001–10	0.22

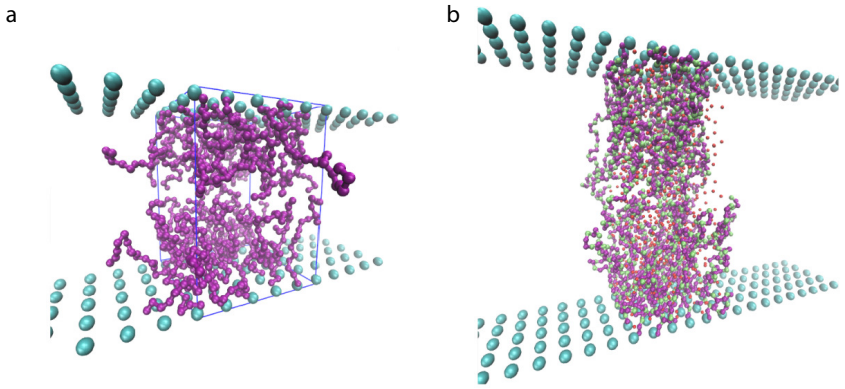

Fig. 1 The snapshots of the neutral brushes (a) and charged brushes (b) represented by the CPK model. The neutral monomers, the fixed-end monomers, the cation monomers, and the anion counterions are represented as pink, cyan, green, and red balls, respectively. Only one box of brushes is shown, and the other box is represented by the fixed end-monomers at the walls. See the text in the paper for details.

https://doi.org/10.1007/s10118-024-3151-3

$$U_{\text{Coul}}(r) = k_{\text{B}}Tl_{\text{B}}\frac{q_i q_j}{r} \quad (4)$$

where q_i is the charge valence of the i^{th} particle being equal to ±1 for monovalent charges. The Bjerrum length $l_{\text{B}} = e^2/(4\pi\varepsilon_0\varepsilon k_{\text{B}}T)$determines the strength of the electrostatic interactions with ε_0 being the vacuum permittivity. The long-range Coulomb interaction in the 2-dimensional slab geometry is treated by 3-dimension Ewald summation with correction term. The electrostatic interactions between all charges in the simulation box and all of their periodic images were computed by the particle mesh Ewald algorithm implemented in the LAMMPS software packages.[15]

To study the system in equilibrium at constant temperature, we use stochastic molecular dynamics. The motion of particle i at position $r_i(t)$ follows the Langevin equation,

$$m\frac{\mathrm{d}^2 r_i}{\mathrm{d}t^2} = -\nabla_i U - \Gamma\frac{\mathrm{d}r_i}{\mathrm{d}t} + W_i(t) \quad (5)$$

where all particles have the same mass m in our simulation, Γ is the friction constant which is determined by the coupling of the particles to the heat bath, and $U = U_{\text{LJ}} + U_{\text{FENE}} + U_{\text{Wall}} + U_{\text{Coul}}$ is the potential energy. The system is held at thermal equilibrium by a Gaussian random force $W_i(t)$ with zero average $\langle W_i(t)\rangle = 0$ and autocorrelation function related to friction constant Γ by the fluctuation dissipation theorem,

$$\langle W_i(t)\cdot W_j(t')\rangle = 6k_{\text{B}}T\Gamma\delta_{ij}\delta(t-t') \quad (6)$$

The parameters used in the simulation are m=1, $T = 1.0\varepsilon_{\text{LJ}}/k_{\text{B}}$ and $\Gamma = 1.0m/\tau_{\text{LJ}}$ with the LJ time $\tau_{\text{LJ}} = \left(m\sigma^2/\varepsilon_{\text{LJ}}\right)^{1/2}$. A velocity Verlet algorithm was used to integrate the equation of motion (Eq. 5) with a time step equal to $\Delta t = 0.01\tau_{\text{LJ}}$ for the shearing velocity $< 0.1\sigma/\tau_{\text{LJ}}$ and $\Delta t = 0.005\tau_{\text{LJ}}$ for the shearing velocity $\geq 0.1\sigma/\tau_{\text{LJ}}$.

The initial state for chains was chosen to be straight configuration with a line of neighboring counterions. The configurations at several selected values of separation D are saved. The approach to equilibrium was monitored by the relaxation of the end-to-end vector of chains. The number of MD steps at the fixed separation D is chosen to be 2–10 relaxation times of the end-to-end vector of chains in x-y directions depending on the system parameters. Shear is imposed by moving the two grafted surfaces oppositely in x-directions at a fixed velocity V/2. To avoid biasing of the particle velocity profile in the shear direction by the Langevin thermostat, only y and z-components of the velocity are coupled to the thermostat.

The normal and shear forces were determined from the LJ short-range force experienced by both top and bottom walls from monomers and counterions, and FENE bond force at the grafted end of the chains. Alternatively the normal and shear forces were evaluated from the stress tensor,

$$P_{\alpha\beta} = \frac{1}{V}\left[\sum_{i=1}^{N_{\text{tot}}}\langle mv_{i\alpha}v_{i\beta}\rangle - \sum_{i=1}^{N_{\text{tot}}}\sum_{j=i+1}^{N_{\text{tot}}}\langle\nabla U_{ij\alpha}\cdot(r_{ij\beta} - R_{n\beta})\rangle\right] \quad (7)$$

where indexes α and β denote the Cartesian components, v_i is the corresponding velocity components of a particle i, and R_{n} is the two-dimensional transitional vector over the periodic images of the simulation box. We use Eq. (7) for our calculations of normal pressure P_{zz} and shear stress P_{xz}.

Our model may be compared with the most studied polyelectrolyte brushes, such as poly(styrenesulfonate) with sodium counterions (Na-PSS) in aqueous solution. Na-PSS has one charged group per monomer, with a monomer length $b \cong 0.97\sigma \cong 3$Å. In aqueous solution, the Bjerrum length is $l_{\text{b}} \cong 7$ Å, and thus our model of brushes may be mapped to Na-PSS with counter length around 12 nm.

RESULTS AND DISCUSSION

Neutral Brushes

Normal forces and shearing forces between two neural brushes

Assuming that hydrodynamic interactions are screened on the length scales on the order of correlation length ξ, the shear stress of the brushes in semidilute solutions are estimated by the number of correlation blobs per unit area in the regime of linear response where $\dot{\gamma} < \frac{1}{\tau}$. The transition shear rate $\dot{\gamma}^*$ at crossover can be estimated by the relaxation time of brush chainτ as $\dot{\gamma}^* \approx \frac{1}{\tau}$. For partially penetrating brushes, the friction force is contributed by all of the correlation blobs in the interpenetration zone. The density number of correlation blobs is $\frac{\delta}{\xi^3}$, and the force contribution of each blob can be estimated by the Stokes law as $V\eta_{\text{s}}\xi$. Thus, the shear stress is given by:[6]

$$P_{xz} \approx V\eta_{\text{s}}\frac{\delta}{\xi^2} \approx \dot{\gamma}\eta_{\text{s}}\frac{D\delta}{\xi^2} \quad (8)$$

and for fully penetrating brushes, $\delta \approx D$, and the shear stress is given by:

$$P_{xz} \approx \dot{\gamma}\eta_{\text{s}}\frac{D^2}{\xi^2} \quad (9)$$

where η_{s} is the solvents viscosity, δ is the thickness of interpenetrating brushes. Because of $\xi \approx b/\varphi$ in the neutral θ solutions, the scaling theory predicts that $P_{xz} \approx \dot{\gamma}\eta_{\text{s}}\frac{\delta}{D}$ for the semidilute θ solutions.

Fig. 2 shows the dependence of the shear stress P_{xz} of neutral brushes on the shear rate $\dot{\gamma}$ for the different separations D for the brushes of $N = 20$ and $\rho = 0.11\sigma^{-2}$. Our simulation results, shown in Fig. 2(a), confirm that with the increase of the shear rate, the shear stress P_{xz} of the brushes cross over from the regime linear response to the non-linear response regime, in which the shear stress shows weaker dependence on the shear rate. For the higher shear rate above the transitional shear rate $\dot{\gamma}^*$, the power law of the shear stress scaling shear rate as $P_{xz} \sim \dot{\gamma}^{0.54}$ are reported by lots of studies.[7,12] The nonlinear response of bushes is not the focus of this paper, therefore we will not discuss the results here.

Usually, the normal stress P_{zz} by the walls is dominated by osmotic pressure Π of correlation blobs for the neutral brushes. The scaling theory predicts that

$$P_{zz} \approx \Pi \approx \frac{kT}{\xi^3} \approx \frac{kT}{b^3}\varphi^3 \sim D^{-3} \quad (10)$$

Our simulation results in Fig. 3(a) show that the normal stress is almost independence on the shear rate except in very high shear rate. However, the dependence of normal stress on the separation distance is deviated quantitatively from the scaling prediction of $P_{zz}(0) \sim D^{-3}$. Our simulation results at strongly compressed regime shows a stronger dependence as $P_{zz}(0) \sim D^{-4\pm0.2}$, as shown in Fig. 3(b). The reason may be that

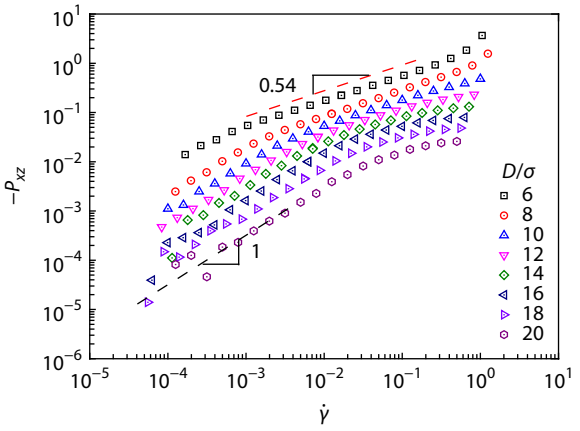

Fig. 2 Dependence of shear stress P_{xz} on the shear rate $\dot{\gamma}$ for the neutral brushes.

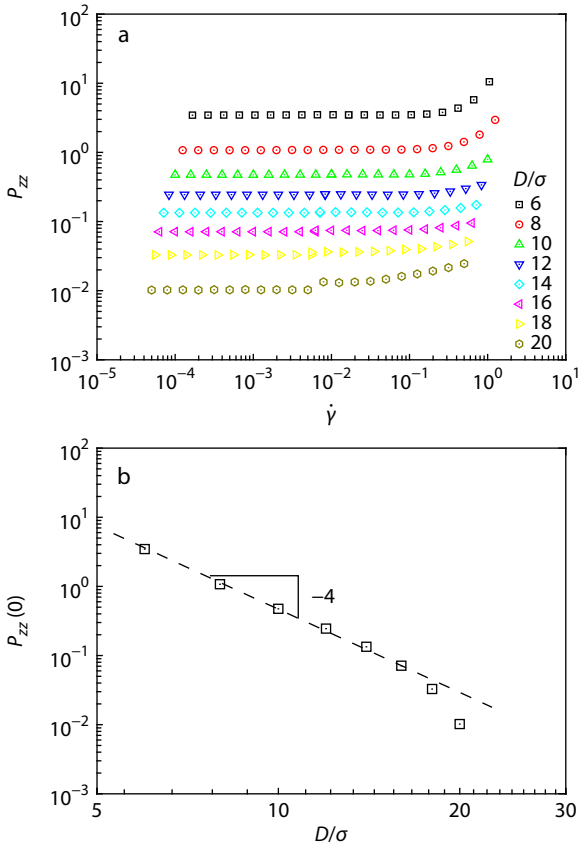

Fig. 3 (a) Dependence of normal stress P_{zz} on the shear rate $\dot{\gamma}$ at different separation distance D for the neutral brushes; (b) Dependence of normal stress $P_{zz}(0)$ at zero shear rate on separation distance D for the neutral brushes.

the brushes cross over to the entanglements and/or the glass transition in the strongly compressed regime with the decreasing of separation.

Effective viscosities between two neural brushes

The effective viscosity is defined as the ratio of measured shear stress and externally imposed effective rate $\eta \equiv \frac{P_{xz}}{\dot{\gamma}}$. In partially interpenetrating charged brushes, the effective viscosity is predicted as,

$$\eta \approx \eta_s D\frac{\delta}{\xi^2} \sim \eta_s \frac{\delta}{D} \tag{11}$$

and in the fully interpenetrating charged brushes, the effective viscosity is predicted as,

$$\eta \approx \eta_s \frac{D^2}{\xi^2} \sim \eta_s \tag{12}$$

The scaling law in Eqs. (11) and (12) predict a very weak dependence of effective viscosity of brushes on the separation. In Fig. 4(a), the effective viscosity of neutral brushes η_n is plotted as a function of shear rate at different separation D between the two neutral brushes for grafting density $\rho = 0.11\sigma^{-2}$. The results normalized by the relaxation time and the zero-shear viscosity are shown in Fig. 4(b). The inset of Fig. 4(b) shows that the effective viscosity at crossover is scaling as $\eta_n^* \sim D^{-3.5\pm0.5}$ for the strongly compressed neutral brushes simulated in this study. Similar to the results of the normal force, the dependence of shear force and effective viscosity are also stronger that the scaling predictions given in Eqs. (11) and (12).

Friction coefficients between two neutral brushes

Friction coefficient is conventionally defined as the ratio of fric-

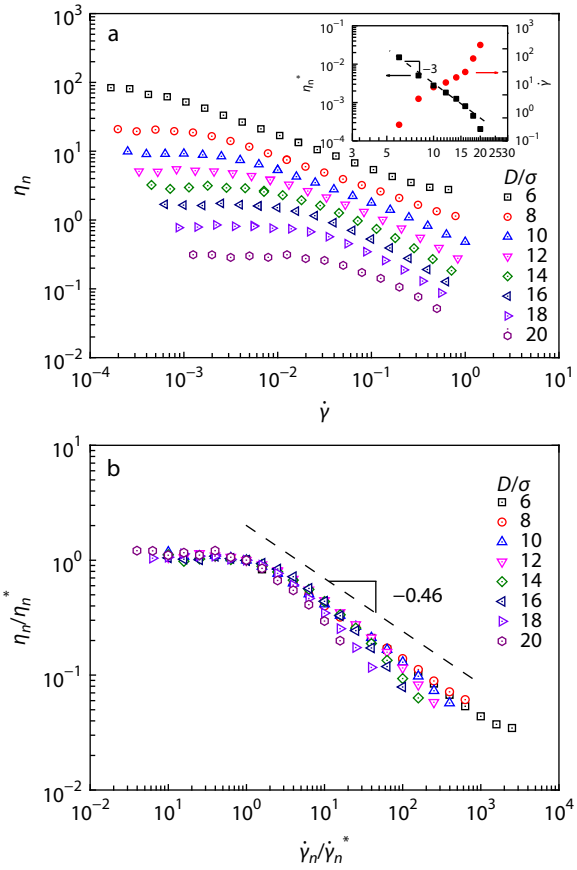

Fig. 4 Effective viscosity of neutral brushes η_n as a function of shear rate at different separation D between the two brushes for grafting density $\rho = 0.11\sigma^{-2}$. (a) Raw data and (b) reduced by the transitional shear rate $\dot{\gamma}^*$ and effective viscosity η_n^*. The inset shows the dependence of the transitional shear rate $\dot{\gamma}^*$ and effective viscosity η_n^* on the separation D.

https://doi.org/10.1007/s10118-024-3151-3

tion to normal force, or the ratio of shear stress to the pressure in our simulations:

$$\mu = \frac{-P_{xz}}{P_{zz}} \tag{13}$$

The lubrication properties of the brushes depend on friction coefficients in the different regimes. The main focus of the paper is the neutral/polyelectrolyte brushes in the strongly compressed regime, in which the normal force gives a dependence of separation D as $P_{zz} \sim D^{-4}$ (Fig. 3b). Fig. 5 shows our simulation results of the friction coefficients as a function of shear rate between the two brushes at different separations D for grafting density $\rho = 0.11\sigma^{-2}$. Because the friction coefficient is proportional to the shear rate in the linear regime, the better parameter to describe the lubrication properties is the ratio of friction coefficient to the shear rate at zero-shearing $\lim_{\dot{\gamma}\to 0}\mu/\dot{\gamma}$. The ratio of friction coefficient to the shear rate at zero-shearing are shown in the inset of Fig. 5. The strongly compressed contribution of polymer to normal force and shear force cancels each other with decreasing of separation, therefore, the ratio of friction coefficients to the shear rate shows a weaker dependence on the separation comparing the effective viscosity in our simulations, which is about scaling as $\lim_{\dot{\gamma}\to 0}\mu/\dot{\gamma} \sim D^{1/3}$ in our simulations (see inset of Fig. 5). The result confirms the lubrication properties of neutral bushes that the friction decreases with the load increases at the same shear rate.

Charged Brushes

Normal forces and shearing forces between two PE brushes

The similar results of normal force and shear force, effective viscosity, and the frictions coefficients are given in the section. Fig. 6 shows the dependence of shear stress P_{xz} charged brushes on the shear rate $\dot{\gamma}$ for the different separations D for the brushes of $N = 40$ and $\rho = 0.11\sigma^{-2}$.

In contrast to neutral brushes, the normal pressure felt by the surfaces is dominated by the conterions. At stronger compressions, the normal pressure is produced by the osmotic pressure of counterions uniformly distributed between the

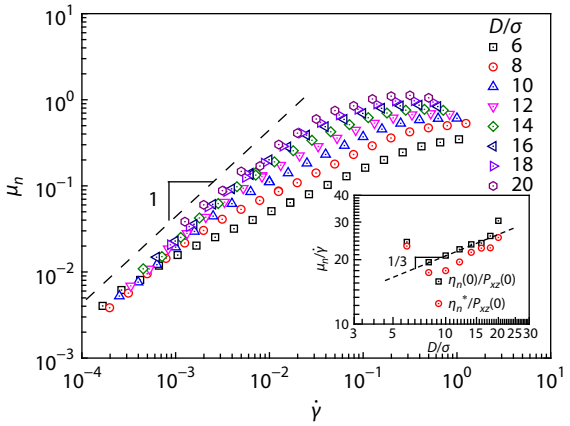

Fig. 5 Friction coefficients as a function of shear rate between the two neural brushes at different separations D for grafting density $\rho = 0.11\sigma^{-2}$. The inset shows the dependence of $\lim_{\dot{\gamma}\to 0}\mu/\dot{\gamma}$ on the separation D.

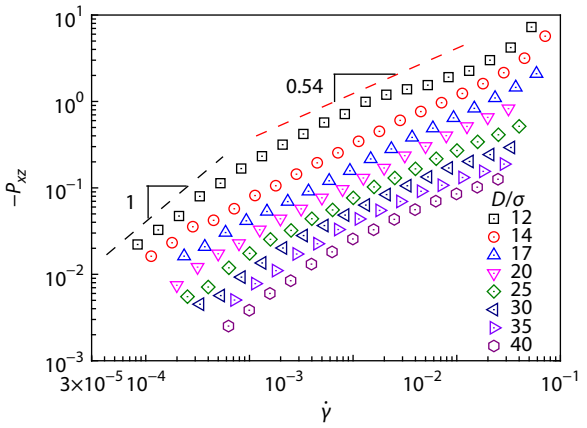

Fig. 6 Dependence of shear stress P_{xz} on the shear rate $\dot{\gamma}$ for the charged brushes.

two grafted surfaces,

$$P_{ni} = k_B T c_i \approx \frac{k_B TfN\rho}{D} \tag{14}$$

The polymer contribution of normal force at higher compression is similar to the pressure in the neutral brushes,

$$P_{np} \approx \frac{k_B T}{b^3}\left(\frac{b^3 N\rho}{D}\right)^{3\nu/(3\nu-1)} \tag{15}$$

The dependence of the normal stress P_{zz} on the shear rate $\dot{\gamma}$ at different separation distance D for the charged brushes, as well as the zero-shearing normal stress on the separation of compressed polyelectrolyte brushes is shown in Fig. 7. Our simulation results shown in Fig. 7 confirm the predictions given in Eqs. (14) and (15) that the normal pressure of charged brushes is stronger than that of neutral brushes in the larger separations. With the decrease of the separation, the charged brushes cross over to the compressed quasi-neutral brush regime, in which the normal pressure shows stronger dependence on plate separation at high compression. The charged brushes show the similar power law of $P_{zz} \sim D^{-4\pm0.2}$ observed in the neutral bushes in the lower limit of the separation, which indicates that the polymer contribution dominates the normal pressure in the regime.

Effective viscosities between two PE brushes

In Fig. 8(a), the effective viscosity of charged brushes η_c is plotted as a function of shear rate at different separation D between the two brushes for grafting density $\rho = 0.11\sigma^{-2}$. The results normalized by the relaxation time and the zero-shear viscosity are shown in Fig. 8(b). In the scaling theory, Eqs. (11) and (12) still work for the shear force of charged brushes, which predict a very weak dependence of effective viscosity of brushes on the separation. The inset of Fig. 8(b) shows that the effective viscosity at crossover is scaling as $\eta_n^* \sim D^{-2.5\pm0.5}$ for the strongly compressed charged brushes simulated in this study. Similar to the results of the neutral brushes, the dependence of shear force and effective viscosity are also stronger that the scaling predictions given in Eqs. (11) and (12).

Friction coefficients between two PE brushes

Fig. 9 shows our simulation results of the friction coefficients as a function of shear velocity between the two brushes at different separations D for grafting density $\rho = 0.11\sigma^{-2}$. The simula-

https://doi.org/10.1007/s10118-024-3151-3

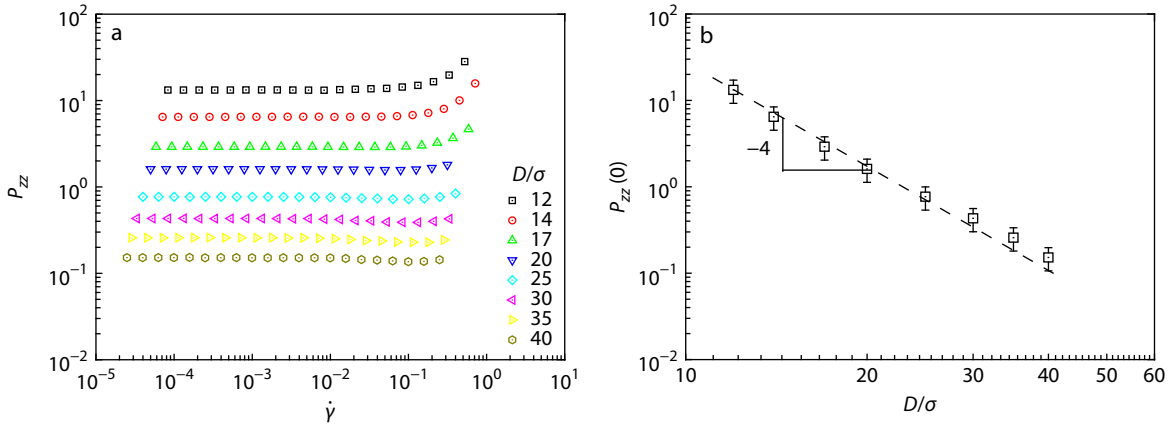

Fig. 7 Dependence of the normal stress P_{zz} on the shear rate $\dot{\gamma}$ (a) and separation distance D (b) for the charged brushes.

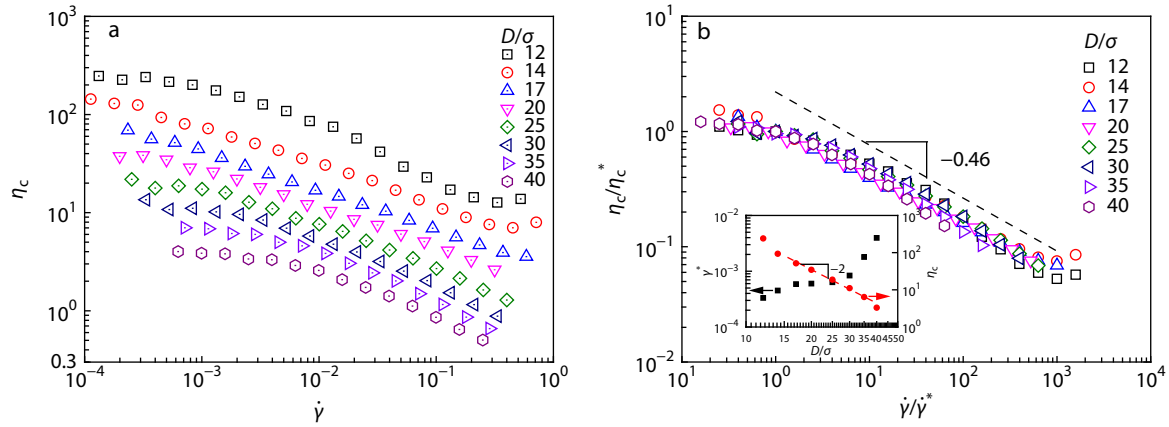

Fig. 8 Effective viscosity of charged brushes as a function of shear rate at different separation D between the two brushes for grafting density $\rho = 0.11\sigma^{-2}$. (a) Raw data, (b) reduced by the transitional shear rate $\dot{\gamma}^*$ and effective viscosity η_n^*. The inset shows the dependence of the transitional shear rate $\dot{\gamma}^*$ and effective viscosity η_n^* on the separation D.

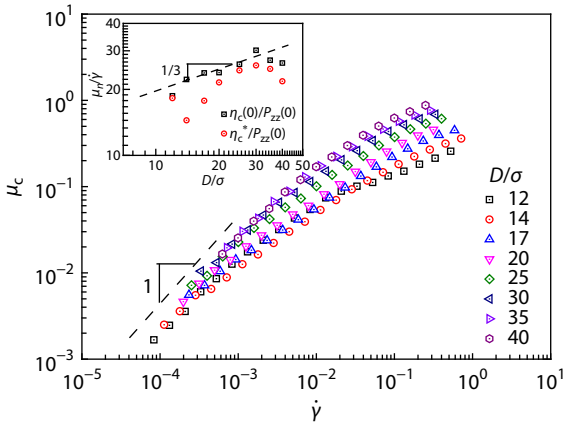

Fig. 9 Friction coefficients as a function of shear rate between the two charged brushes at different separations D for grafting density $\rho = 0.11\sigma^{-2}$. The inset shows the dependence of $\lim_{\dot{\gamma}\to 0}\mu/\dot{\gamma}$ on the separation D.

tion results confirm that the electrostatic interaction is screened in the strongly compressed polyelectrolyte brushes, and shows the similar lubrication properties as we observed in the strongly compressed neutral brushes. However, our simulations could not compare the results with the scaling predictions quantitatively. The inset of Fig. 9 shows the ratio of friction coefficient to the shear rate at zero-shearing $\lim_{\dot{\gamma}\to 0}\mu/\dot{\gamma}$ by two algorithms. Both results of the ratio of friction coefficient to the shear rate at zero-shearing $\lim_{\dot{\gamma}\to 0}\mu/\dot{\gamma}$ show there is a maximum as increasing of the separation of polyelectrolyte brushes, which are not observed in the neutral brushes. The results imply that the lubrication properties of charged bushes get worse at a critical load, but will get better with the increasing with the load at the same shear rate. However, the results of two algorithms are only consistent to the each other qualitatively. We will leave this problem in the future studies.

CONCLUSIONS

We present the results of molecular dynamics simulations of steady shear between a pair of neutral or charged brushes in the strongly compressed regime. Our simulation results for the normal forces of compressed polyelectrolyte brushes are stronger than the predictions of the scaling model in the semidilute regime. The results of shear forces for the separation dependence are in qualitative agreement with the predictions of the scaling model. The ratio of friction coefficients to the shear rate shows a maximum as increasing of the separation of polyelec-

https://doi.org/10.1007/s10118-024-3151-3

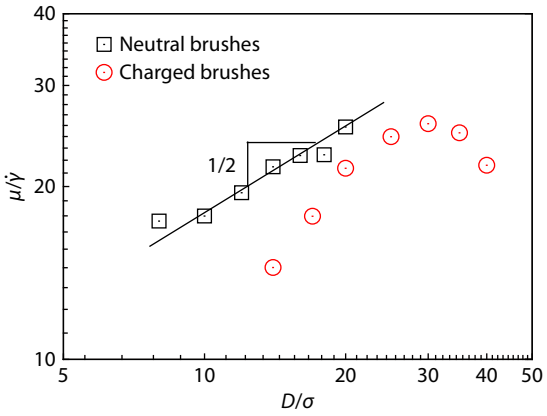

Fig. 10 Comparison of friction coefficients at the same shear rate as a function of separation between a pair of neutral and charged brushes. The definition of $\lim_{\dot{\gamma}\to 0}\mu/\dot{\gamma} = \eta^*/P_{zz}(0)$ is used and the pointes are replotted by the insets of Figs. 5 and 9. The dash line with slope 1/2 is for the guide of eyes.

trolyte brushes between the threshold of brush chain contact and fully interpenetrated brushes. The velocity-dependent friction coefficient between two partially interpenetrated polyelectrolyte brushes is weakly dependent of the separation distance in the regime of strong compression for both of neutral and the charged brushes.

Fig. 10 shows the comparison of friction coefficients at the same shear rate as a function of separation between a pair of neutral and charged brushes. Both of neutral and charged brushes show the lubrication properties that the friction coefficient decreases with the separation decreases at enough larger loads. However, a maximum of friction coefficients is observed for polyelectrolyte brushes, which is in contrast to the neutral brushes with monotonical dependence. The results imply that the lubrication properties of charged bushes get worse at a critical load, but will get better with the increasing of the load at the same shear rate.

Conflict of Interests

The authors declare no interest conflict.

Data Availability Statement

The data that support the findings of this study are available from the corresponding author upon reasonable request. The author's contact information: qiliao@iccas.ac.cn.

ACKNOWLEDGMENTS

This work was financially supported by the National Natural Science Foundation of China (Nos. 21574139 and 21973103).

REFERENCES

1 Rubinstein, M.; Colby, R. H. *Polymer Physics*. Oxford University Press, Oxford, **2003**.
2 Chen, M.; Briscoe, W. H.; Armes, S. P.; Klein, J. Lubrication at physiological pressures by polyzwitterionic brushes. *Science* **2009**, *323*, 1698.
3 Raviv, U.; Giasson, S.; Kampf, N.; Gohy, J. F.; Jerome, R., Klein, J. Lubrication by charged polymers. *Nature* **2003**, *425*, 163.
4 Raviv, U.; Frey J.; Sak, R.; Laurat, P.; Tadmor, R.; Klein, J. Normal and frictional forces between surfaces bearing polyelectrolyte brushes. *Langmuir* **2002**, *18*, 7482.
5 Sokoloff, J. B. Theory of friction between neutral polymer brushes. *Macromolecules* **2007**, *40*, 4053.
6 Zhulina, E. B.; Rubinstein, M. Lubrication by polyelectrolyte brushes. *Macromolecules* **2014**, *47*, 5825.
7 Spirin, L.; Galuschko, A.; Kreer, T.; Johner, A.; Baschnagel, J.; Binder, K. Polymer-brush lubrication in the limit of strong compression. *Eur. Phys. J. E* **2010**, *33*, 307.
8 Ou, Y.; Sokoloff, J. B.; Stevens, M. J. Comparison of the kinetic friction of planar neutral and polyelectrolyte polymer brushes using molecular dynamics simulations. *Phys. Rev. E* **2012**, *85*, 011801.
9 Hehmeyer, O. J.; Stevens, M. J. Molecular dynamics simulations of grafted polyelectrolytes on two apposing walls. *J. Chem. Phys.* **2005**, *122*, 134909.
10 Kumar, N. A.; Seidel, C. Interaction between two polyelectrolyte brushes. *Phys. Rev. E* **2007**, *76*, 020801.
11 Carrillo, J. Y.; Russano, D.; Dobrynin, A. V. Friction between brush layers of charged and neutral bottle-brush macromolecules. molecular dynamics simulations. *Langmuir* **2011**, *27*, 14599.
12 Galuschko, A.; Spirin, L.; Kreer, T.; Johner, A.; Pastorino, C.; Wittmer, J.; Baschnage. J. Frictional forces between strongly compressed, nonentangled polymer brushes: molecular dynamics simulations and scaling theory. *Langmuir* **2009**, *26*, 6418.
13 Goujon, F.; Ghouf, F.; Malfreyt, P.; Tildesley, D. J. The kinetic friction coefficient of neutral and charged polymer brushes. *Soft Matter* **2013**, *9*, 2966.
14 Liao, Q.; Carrillo, J. Y.; Dobrynin, A. V.; Rubinstein, M. Rouse dynamics of polyelectrolyte solutions: molecular dynamics study. *Macromolecules* **2007**, *40*, 7671.
15 Thompson, A. P.; Aktulga, H. M.; Berger, R.; Bolintineanu, D. S.; Brown, W. M.; Crozier, P. S.; in 't Veld, P. J.; Kohlmeyer, A.; Moore, S. G.; Nguyen, T. D.; Shan, R.; Stevens, M. J.; Tranchida, J.; Trott, C.; Plimpton, S. J. LAMMPS—a flexible simulation tool for particle-based materials modeling at the atomic, meso, and continuum scales. *Comp. Phys. Commun.* **2022**, *271*, 10817.